Side-Chain Protonation and Mobility in the Sarcoplasmic Reticulum Ca^{2+}-ATPase: Implications for Proton Countertransport and Ca^{2+} Release

K. Hauser* and A. Barth†

*Institut für Biophysik, Johann Wolfgang Goethe-Universität Frankfurt, 60438 Frankfurt am Main, Germany; and †Department of Biochemistry and Biophysics, Stockholm University, Arrhenius Laboratories for Natural Sciences, SE-106 91 Stockholm, Sweden

ABSTRACT Protonation of acidic residues in the sarcoplasmic reticulum Ca^{2+}-ATPase (SERCA 1a) was studied by multi-conformation continuum electrostatic calculations in the Ca^{2+}-bound state Ca_2E1, in the Ca^{2+}-free state E2(TG) with bound thapsigargin, and in the E2P (ADP-insensitive phosphoenzyme) analog state with MgF_4^{2-} E2(TG+MgF_4^{2-}). Around physiological pH, all acidic Ca^{2+} ligands (Glu^{309}, Glu^{771}, Asp^{800}, and Glu^{908}) were unprotonated in Ca_2E1; in E2(TG) and E2(TG+MgF_4^{2-}) Glu^{771}, Asp^{800}, and Glu^{908} were protonated. Glu^{771} and Glu^{908} had calculated pK_a values larger than 14 in E2(TG) and E2(TG+MgF_4^{2-}), whereas Asp^{800} titrated with calculated pK_a values near 7.5. Glu^{309} had very different pK_a values in the Ca^{2+}-free states: 8.4 in E2(TG+MgF_4^{2-}) and 4.7 in E2(TG) because of a different local backbone conformation. This indicates that Glu^{309} can switch between a high and a low pK_a mode, depending on the local backbone conformation. Protonated Glu^{309} occupied predominantly two main, very differently orientated side-chain conformations in E2(TG+MgF_4^{2-}): one oriented inward toward the other Ca^{2+} ligands and one oriented outward toward a protein channel that seems to be in contact with the cytoplasm. Upon deprotonation, Glu^{309} adopted completely the outwardly orientated side-chain conformation. The contact of Glu^{309} with the cytoplasm in E2(TG+MgF_4^{2-}) makes this residue unlikely to bind lumenal protons. Instead it might serve as a proton shuttle between Ca^{2+}-binding site I and the cytoplasm. Glu^{771}, Asp^{800}, and Glu^{908} are proposed to take part in proton countertransport.

INTRODUCTION

The Ca^{2+}-ATPase (SERCA 1a) (1) couples the transport of two Ca^{2+} ions across the sarcoplasmic reticulum (SR) membrane to the hydrolysis of one molecule of ATP (2–5). Associated with Ca^{2+} transport is proton countertransport from the SR to the cytoplasm (6–8). Binding of two cytosolic Ca^{2+} to the Ca^{2+}-ATPase in the E2 or E1 state (E2/E1 → Ca_2E1) releases H^+ into the cytoplasm and enables ATP to phosphorylate Asp^{351} of the ATPase. Subsequently, the phosphoenzyme converts from an ADP-sensitive form (Ca_2E1P) to an ADP-insensitive form (E2P). Phosphoenzyme conversion is associated with Ca^{2+} release toward the SR lumen against the concentration gradient. E2P picks up protons from the lumenal side of the membrane that are countertransported and released to the cytoplasmic side upon Ca^{2+} binding. Proton countertransport is reduced at high lumenal pH (9).

Binding of the countertransported protons is thought to take place at acidic residues in the Ca^{2+}-binding sites (6,7,10–13). The binding sites contain four carboxyl groups: Glu^{309} (Ca^{2+}-binding site II), Glu^{771} (site I), Asp^{800} (sites I and II), and Glu^{908} (site I) (14,15). Mutagenesis studies have indicated a possible involvement of Glu^{309} (16,17), Glu^{771} (18), and Asn^{796} (19) in proton or H_3O^+ binding and proton countertransport.

Most acidic Ca^{2+} ligands are buried in the Ca^{2+}-free states (20–24) without compensating positive charges nearby: in an E2P analog structure obtained with MgF_4^{2-}, the closest positively charged residue is His^{944} at 9.7 Å distance to Asp^{800}. Thus the carboxyl groups are likely protonated in the Ca^{2+}-free states, and direct evidence for protonation of carboxyl groups upon Ca^{2+} release from the unphosphorylated and phosphorylated ATPase has been obtained by infrared spectroscopy (25–30).

In line with this, previous continuum electrostatic calculations on the structure of E2(TG+BHQ) (23)—Ca^{2+}-free ATPase with thapsigargin (TG) and 2,5-di-*tert*-butyl-1,4-dihydroxybenzene (BHQ) bound—have indicated that all of these residues are protonated at least at pH 6, whereas all except Glu^{908} are unprotonated in Ca_2E1 (31). It was suggested (23) that all acidic Ca^{2+} ligands are protonated by lumenal protons, meaning that all participate in proton countertransport except for Glu^{908}, which does not lose its proton upon Ca^{2+} binding between pH 6 and 7. Protonation of Glu^{58} by Glu^{309} could possibly reduce the number of countertransported protons (23), which would also exclude Glu^{309} from being a proton-countertransporting residue. However, these calculations do not reproduce the reduced Ca^{2+}/H^+ stoichiometry proton countertransport at high pH (9) because Glu^{309}, Glu^{771}, and Asp^{800} remain essentially protonated in E2(TG+BHQ) between pH 6 and 8 and Glu^{908} has a similar pK_a in Ca_2E1 and E2(TG+BHQ). Since proton countertransport is reduced by increasing the lumenal pH from 6 to 8 (9), the participating residues should be less protonated at high pH.

Several other Ca^{2+}-free structures have been published (20–22,24,32). The Ca^{2+}-free structures differ as to whether

Submitted March 26, 2007, and accepted for publication July 5, 2007.

Address reprint requests to K. Hauser, Institut für Biophysik, Johann Wolfgang Goethe-Universität Frankfurt, Max-von-Laue-Str.1, 60438 Frankfurt am Main, Germany. Tel.: 49-69-798-46407; Fax: 49-69-798-46421; E-mail: hauser@biophysik.uni-frankfurt.de.

Editor: Peter Tieleman.

0006-3495/07/11/3259/12 $2.00

doi: 10.1529/biophysj.107.109363

phosphate mimics have been used to stabilize analogs of E2P (21,22,32) and whether TG (20–22,24), TG and BHQ (23), or cyclopiazonic acid (CPA) (32) were used to stabilize the structures. Generally, the structures are similar in the transmembrane region and in particular around the Ca^{2+}-binding sites (21–24), with the exception of the structures with CPA, which indicate plasticity of transmembrane helices M1–M3 (32).

In this study, we investigated the effects of side-chain flexibility on the calculated pK_a values of the carboxyl ligands in different enzyme conformations. Side-chain conformations and ionization changes are sampled in the same simulation; thus surrounding dipoles are allowed to change their orientation when a residue changes its charge. This provides more accurate pK_a values (33) than calculations without side-chain flexibility. Changes in side-chain orientations are followed explicitly as a function of pH rather than averaged into the dielectric constant, allowing the unique surrounding of a residue to be taken into account. Indeed, pK_a values calculated with and without side-chain flexibility differed in our calculations, and side-chain flexibility was particularly pronounced for the Ca^{2+} ligand Glu^{309}, which has led to new insight into the role of Glu^{309} in proton countertransport.

To analyze the participation of acidic ligands in proton countertransport, we calculated the pK_a values in crystal structures of several enzyme states: the Ca^{2+}-bound Ca_2E1 state and two Ca^{2+}-free states, E2(TG) and E2(TG+MgF_4^{2-}). The latter is the crystal structure of an E2P analog and is of particular interest since E2P is the intermediate that picks up the lumenal protons. If the carboxyl ligands compete for Ca^{2+} and protons they should be deprotonated in the Ca^{2+}-bound state, Ca_2E1, and protonated in the Ca^{2+}-free states, E2(TG) and E2(TG+MgF_4^{2-}), at physiological pH. If they are additionally involved in proton countertransport, they should deprotonate in the Ca^{2+}-free states at high pH.

Our calculations with side-chain flexibility indicate that the Ca^{2+} ligands Glu^{309}, Glu^{771}, Asp^{800}, and Glu^{908} are unprotonated at pH 6 in Ca_2E1. In E2(TG) and E2(TG+MgF_4^{2-}), all of these residues are protonated at pH 6, with the exception of Glu^{309}, which is not protonated in E2(TG). The pK_a value of Glu^{309} depends on the local backbone structure. We find less protonation of the acidic Ca^{2+} ligands at pH 8 than at pH 6, which is in line with the experimental observations (9–11). We propose further that movement of the Glu^{309} side chain triggers Ca^{2+} release via an exit channel between transmembrane helices M1, M2, and M4.

METHODS

MCCE calculations

We performed multiconformation continuum electrostatics (MCCE) calculations (33,34) to obtain the equilibrium distribution of residue ionization and side-chain orientation at a given pH. Calculations were performed with the 2.3 Å crystal structure 1WPG.pdb of an E2P analog, E2(TG+MgF_4^{2-}) (22), the 3.1 Å E2(TG) structure 1IWO.pdb (20), and the 2.5 Å Ca_2E1 structure 1SU4.pdb (3,15). Unless specified otherwise we use ''E2(TG) structure'' for the E2(TG) structure determined by Toyoshima and Nomura (20). In a first set of calculations, crystal water molecules were deleted from the structure file. Cavities large enough to host water molecules were treated in the continuum water approximation using $\varepsilon = 80$. Additional calculations were performed with selected crystal water molecules that are located within 10 Å around Asp^{800}, the ligand of both calcium ions. These are 11 water molecules for the Ca_2E1 structure (1SU4.pdb), 5 for the E2(TG+MgF_4^{2-}) structure (1WPG.pdb), and 0 for E2(TG) (1IWO.pdb).

For our MCCE calculations we used the program version ''mcce_alpha''. Traditional continuum electrostatics considers protein microstates that differ only in residue ionization. Other protein and solvent responses to charges are implicitly included in the continuum dielectric constant. In MCCE, the response of side chains is explicitly taken into account by considering different side-chain orientations (rotamers). Rotamers are constructed systematically by rotating rotatable side-chain bonds with variable angle increment. Conformers are then defined by a specific rotamer, ionization state, and hydrogen positions. Each residue is represented by a set of conformers. All electrostatic interactions are calculated with the program Delphi (35). A dielectric constant of 4 is used for the protein and 80 for the solvent and water-filled cavities. PARSE parameters provide atomic charges and radii (36). Torsion and Lennard-Jones parameters were previously reported (33,34).

Protein microstates are created by choosing one conformer for each residue. These microstates are subjected to Monte Carlo sampling, yielding the occupancy of each conformer according to a Boltzmann distribution as a function of pH. The pK_a values were derived from fitting a titration curve to the fractional residue protonation calculated at each pH varying from 0 to 14. Recent MCCE analysis on proteins and details of the method can be found (e.g., 37–41).

The transmembrane domain with the Ca^{2+}-binding sites was assigned according to SCOP (the Structural Classification of Proteins Database) classifications (42). For residues in the transmembrane domain (residues 1–124; 240–343; 751–994), rotamers were generated around each rotatable bond with an angle increment of 60°; for all other residues the increment was 180°. Thus the transmembrane residues were represented by a larger number of rotamers in the calculations than the residues in the cytoplasmic domains to balance more precise pK_a calculations with a reasonable number of conformers and computation time.

The inhibitor TG was kept in the E2(TG) and E2(TG+MgF_4^{2-}) structure file and treated as neutral cofactor because it is not present under physiological conditions. ADP, Na^+, MgF_4^{2-}, and Mg^{2+} in the cytoplasmic domains were removed in E2(TG+MgF_4^{2-}) because they are far away from the transmembrane region where proton countertransport takes place, at least 32 Å away from the binding sites.

In the calculations of the Ca_2E1 state, all Ca^{2+} ligands were treated as fixed rotamers to account for a correct Ca^{2+} coordination geometry. This was necessary because the ion-ligand distances are so short that the strong interactions are not correctly reproduced by classical force field approaches as implemented in MCCE. As a consequence, Ca^{2+} ligands turned away from Ca^{2+} in unrestrained MCCE calculations. In E2(TG+MgF_4^{2-}) and E2(TG), all residues including the ligands were treated as multiple conformers.

The calculations were performed without a membrane model. Control calculations of E2(TG+MgF_4^{2-}) with a POPC (1-palmitoyl-2-oleoyl-*sn*-glycero-3-phosphocholine) membrane confirmed that the impact on the pK_a values of the carboxyl ligands is marginal (≤ 0.3 ΔpK_a units) as expected since the binding site residues are buried in the protein.

Estimation of the strength of backbone interactions around Glu^{309}

To judge whether Glu^{309} has predominantly a low or a high pK_a value, we studied whether the Glu^{309} conformers of E2(TG) or E2(TG+MgF_4^{2-}) are energetically more favorable. For this, interactions of the Glu^{309} side chain,

which are included in the ΔG values in Table S1 of the Supplementary Material, and interactions of the local backbone around Glu^{309} need to be considered and compared for the two states. Some of the intrabackbone interactions are not obtained from MCCE calculations and are estimated here.

The local backbone structure around Glu^{309} is different in E2(TG) and E2(TG+MgF_4^{2-}). In E2(TG), the backbone carbonyl group of Asn^{796} is close to the carbonyl group of Glu^{309} of E2(TG) but close to the NH group of Gly^{310} in E2(TG+MgF_4^{2-}). Thus, the energy difference between E2(TG) and E2(TG+MgF_4^{2-}) due to the local backbone structure around Glu^{309} contains two contributions: i) repulsion between Glu^{309} and Asn^{796} in E2(TG), and ii) attraction between Glu^{309} and Gly^{310} in E2(TG+MgF_4^{2-}). The former is included in ΔG_{pol} of Glu^{309} and does not need to be considered separately. The latter cannot be obtained from MCCE calculations, and we thus estimated the hydrogen-bond energy. We note that this estimation is not implemented in the MCCE calculations. The strength of the hydrogen bond between Gly^{310} NH and Asn^{796} CO in E2(TG+MgF_4^{2-}) was estimated as follows: According to distance- and angle-dependent calculations of the hydrogen-bond energy between *N*-methylacetamide dimers with the CHARMM22 force field (43), the hydrogen-bond energy in the E2(TG+MgF_4^{2-}) structures is 8–12 kJ/mol at $\varepsilon = 1$, which corresponds to 0.4–0.5 ΔpK_a units at $\varepsilon = 4$. 1 ΔpK_a unit = 5.7 kJ/mol = 1.36 kcal/mol = 58 meV. The nonlinearity of the hydrogen bond positions it on the slope of the low energy valley of the hydrogen-bond energy surface.

Distance measurements, surface calculations, and illustrations

Structures were analyzed using Swiss-Pdb Viewer and Protein Explorer (44). Distance measurements and surface calculations for the Ca^{2+} release path section were done with structures to which hydrogen atoms had been added. Figures were prepared with PyMOL, Rastop, and Swiss-PdbViewer.

RESULTS AND DISCUSSION

Protonation of Ca^{2+} ligands

We performed MCCE to study protonation of the acidic Ca^{2+} ligands in the ATPase states Ca_2E1, E2(TG) and E2(TG+MgF_4^{2-}), the E2P analog with MgF_4^{2-}. The structure of a second E2P analog (with AlF_4^-) has been published (21). Of the two E2P analog structures we chose the MgF_4^{2-} structure because of its better resolution. The E2P analog structures are considered to represent a transition state (AlF_4^-) or product state of E2P dephosphorylation (MgF_4^{2-}). A better mimic of E2P seems to be the beryllium fluoride analog in the absence of TG because its Ca^{2+}-binding sites are accessible from the lumenal side of the SR (45). However, a crystal structure is not yet available for this beryllium fluoride complex.

The fractional protonation of the acidic Ca^{2+} ligands are shown in Table 1 for Ca_2E1, E2(TG), and E2(TG+MgF_4^{2-}); and Table 2 summarizes their pK_a values. Values derived from the work by Sugita et al. (31) and Obara et al. (23) are given for comparison. Fig. 1 shows representatives of the most occupied conformers of the Ca^{2+} ligands calculated for E2(TG+MgF_4^{2-}) at pH 6.

The protonation state of the acidic Ca^{2+} ligands will strongly depend on the effect of water in the cavity system that is interspersed in the membrane part. Water was modeled as continuum water. Additionally, calculations were carried out with explicitly treated crystal water molecules that are close to the calcium-binding site. The only considerable effect of explicit water is on the pK_a of Asp^{800} in E2(TG+MgF_4^{2-}) where it shifts the pK_a value up by 0.8 ΔpK_a units. This is still less than the estimated accuracy of up to ± 1 ΔpK_a unit in MCCE calculations. Unless otherwise mentioned, the values in the text refer to the calculations without explicitly treated water. In the following we will discuss the four acidic residues in the Ca^{2+}-binding sites in more detail.

Glu^{309}: calculated pK_a values

Our pK_a value for Glu^{309} is <0 in Ca_2E1, 4.7 in E2(TG), and 8.4 in E2(TG+MgF_4^{2-}). For Ca_2E1, our result agrees with a recent computational analysis (31) and with disruption of the Ca^{2+}-binding site II upon mutation to Gln (46–50). However, there is a large difference between the value for E2(TG), on the one hand ($pK_a = 4.7$), and those for E2(TG+MgF_4^{2-}) ($pK_a = 8.4$) obtained here and E2(TG+BHQ) ($pK_a > 8$) obtained by Obara et al. (23), on the other hand. We attribute this to the different local backbone structure around Glu^{309} as shown in Fig. 2. The amide oxygen faces outward in E2(TG+MgF_4^{2-}) and inward in E2(TG) and directs the C_α-C_β bond of Glu^{309} differently as shown in Fig. 2 *B*. Backbone structure influences our results because the positions of the backbone atoms and of the C_β atoms are fixed in MCCE calculations. Due to the different direction of the C_α-C_β bond in E2(TG+MgF_4^{2-}) and E2(TG), different Glu^{309} side-chain conformations were generated by MCCE for the two structures which differ in their pK_a values.

Glu^{309}: heterogeneity of side-chain conformation

Despite the different C_α-C_β-bond orientations in the crystal structures of E2(TG) and E2(TG+MgF_4^{2-}), a common result of our MCCE calculations was that the Glu^{309} side chain can orient in opposite directions in both structures. Conformer analysis of the E2(TG+MgF_4^{2-}) calculations showed that at pH 6, over 60% of the occupied conformers adopt side-chain orientations similar to that in the E2(TG+MgF_4^{2-}) crystal structure and are protonated predominantly at the $O_{\varepsilon 2}$ oxygen. The side chain is oriented inward toward the other Ca^{2+} ligands. The remaining 40% of conformers adopt a different conformation, with the carboxyl group rotated around the C_α-C_β bond and pointing away from the Ca^{2+}-binding sites and toward a channel to the cytosol as illustrated in Fig. 1.

This outward orientation resembles that in the E2(TG) crystal structure as shown in Fig. 2. The outwardly oriented rotamer of E2(TG+MgF_4^{2-}) is occupied to 100% when Glu^{309} deprotonates at high pH. Heterogeneity of the Glu^{309} side-chain conformation was also observed in the calculations with E2(TG). Here, the predominant orientation of protonated Glu^{309} was outward (86% at pH 4), but inward orientations were adopted by a significant minority (14% at pH

TABLE 1 Calculated fractional protonation in dependence of pH of the carboxyl groups that constitute the Ca^{2+}-binding sites

A															
pH	0	1	2	3	4	5	6	7	8	9	10	11	12	13	14
Glu^{309}*															
Ca_2E1	0	0	0	0	0	0	0	0	0	0	0	0	0	0	0
$E2(TG+MgF_4^{2-})$	1	1	1	1	1	1	0.98	0.94	0.73	0.22	0.02	0	0	0	0
E2(TG)	1	1	0.99	0.93	0.76	0.41	0.11	0	0	0	0	0	0	0	0
Glu^{771}															
Ca_2E1	0.02	0.01	0.02	0.01	0.01	0	0	0	0	0	0	0	0	0	0
$E2(TG+MgF_4^{2-})$	1	1	1	1	1	1	1	1	1	1	1	1	1	0.98	0.91
E2(TG)	1	1	1	1	1	1	1	1	1	1	1	1	1	1	1
Asp^{800}															
Ca_2E1	0	0	0	0	0	0	0	0	0	0	0	0	0	0	0
$E2(TG+MgF_4^{2-})$	1	1	1	1	0.98	0.93	0.82	0.49	0.19	0.16	0.16	0.10	0.05	0.03	0.03
E2(TG)	1	1	1	1	1	0.99	0.96	0.83	0.44	0.13	0	0.01	0.03	0.02	0.01
Glu^{908}															
Ca_2E1	0.98	0.98	0.94	0.72	0.31	0.09	0.03	0.01	0	0	0	0	0	0	0
$E2(TG+MgF_4^{2-})$	1	1	1	1	1	0.99	0.98	0.93	0.89	0.86	0.84	0.89	0.93	0.94	0.90
E2(TG)	1	1	1	1	1	1	1	0.99	0.95	0.94	1	0.99	0.97	0.97	0.97
B															
pH	0	1	2	3	4	5	6	7	8	9	10	11	12	13	14
Glu^{309}*															
Ca_2E1	0	0	0	0	0	0	0	0	0	0	0	0	0	0	0
$E2(TG+MgF_4^{2-})$	1	1	1	1	1	1	0.99	0.95	0.77	0.29	0.04	0	0	0	0
Glu^{771}															
Ca_2E1	0.01	0.02	0.02	0.01	0.01	0	0	0	0	0	0	0	0	0	0
$E2(TG+MgF_4^{2-})$	1	1	1	1	1	1	1	1	1	1	1	1	1	1	0.98
Asp^{800}															
Ca_2E1	0	0	0	0	0	0	0	0	0	0	0	0	0	0	0
$E2(TG+MgF_4^{2-})$	1	1	1	1	0.99	0.97	0.90	0.63	0.33	0.29	0.25	0.20	0.10	0.07	0.05
Glu^{908}															
Ca_2E1	0.98	0.98	0.95	0.76	0.36	0.11	0.04	0.01	0	0	0	0	0	0	0
$E2(TG+MgF_4^{2-})$	1	1	1	1	1	0.99	0.97	0.89	0.79	0.73	0.75	0.79	0.89	0.90	0.87

The numbers are for one representative calculation. 0 and 1 are shorthand notations for 0.00 and 1.00, respectively. *A*: Water was treated as continuum water; *B*: All crystal water molecules within a 10 Å sphere around Asp^{800} (ligand of both calcium ions) are treated explicitly. The E2(TG) structure does not contain crystal water.

*See text for further discussion.

4). The low population of the inward orientation is due to unfavorable interaction with Ile^{307}. Again, unprotonated Glu^{309} is nearly exclusively oriented outward.

These results demonstrate that MCCE is able to generate inward and outward orientations of Glu^{309} for both structures irrespective of the orientation and local backbone structure in the crystal structure. This implies that outward and inward orientation of Glu^{309} is not dictated by the structural constraints imposed by the protein environment. This finding is not even restricted to the enzyme conformation of the E2 states. Additional calculations with the Ca_2E1P analog structure $Ca_2E1(AlF_x)$ (1WPE.pdb) (22), from which we omitted the

TABLE 2 Calculated pK_a values of the Ca^{2+} ligands

Residue	Ca_2E1		$E2(TG+MgF_4^{2-})$	E2(TG)	E2(TG+BHQ)
	This work implicit water (explicit water)	Previous work, $\varepsilon = 4$ (23)/$\varepsilon = 20$ (31)	This work implicit water (explicit water)	This work implicit water	Previous work (23) $\varepsilon = 4$/$\varepsilon = 20$
Glu^{309}	<0 (<0)	<6 / ~0.5	8.4 (8.6)	4.7	>8 / >8
Glu^{771}	<0 (<0)	<6 / ~3	>14 (>14)	>14	>8 / >8
Asp^{800}	<0 (<0)	<6 / ~−4	7.1 (7.9)	7.9	>8 / >8
Glu^{908}	3.6 (3.7)	>8 / ~7.5	>14 (>14)*	>14	>8 / ~6.5

The first value gives the pK_a obtained with continuum water, the value in parentheses that with explicitly treated water molecules. pK_a values from previous calculations are given for comparison: values for E2(TG+BHQ) and Ca_2E1 at $\varepsilon = 4$ were estimated from the protonation probabilities at pH 6, 7, and 8 given by Obara et al. (23) and those for Ca_2E1 at $\varepsilon = 20$ from the titration curves shown by Sugita et al. (31).

*Glu^{908} deprotonates partially around pH 9.

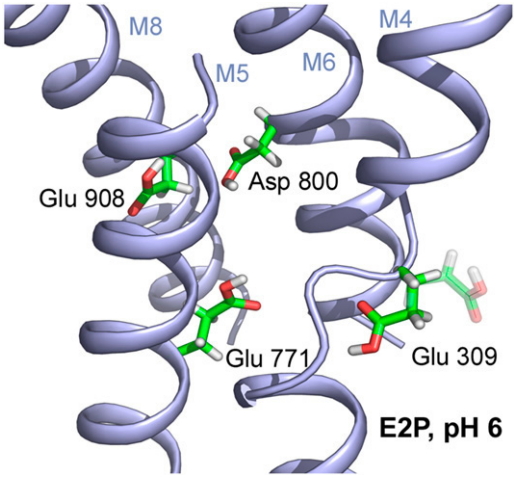

FIGURE 1 Most occupied conformers of the Ca^{2+} carboxyl ligands (Glu^{309}, Glu^{771}, Asp^{800}, Glu^{908}) in the E2(TG+MgF_4^{2-}) state at pH 6. Glu^{309} has two, almost equally occupied conformers at pH 6; the inwardly oriented conformer is similar in structure to the E2(TG+MgF_4^{2-}) crystal structure and represented as solid; the outwardly oriented conformer is shown as transparent. See text for further explanations. M indicates transmembrane helices. Only a part of the transmembrane region of the Ca^{2+}-ATPase is shown. The view is approximately parallel to the membrane. The cytoplasmic side is on the top of the figure, the lumenal side on the bottom. At pH 9, the ionized side chain of Glu^{309} adopts the same conformation as the outwardly oriented conformer at pH 6.

calcium ions, revealed occupation of an outwardly oriented Glu^{309} conformer upon ionization (data not shown), whereas the Glu^{309} side chain in the crystal structure (with Ca^{2+}) is orientated inward. Thus conformational heterogeneity seems to be a genuine property for Glu^{309} in the absence of Ca^{2+}.

Glu^{309} backbone structure and side-chain orientation: survey of crystal structures

There is additional evidence for conformational heterogeneity of Glu^{309} from crystal structures since inward and outward orientations are adopted in different crystal structures of E2P analogs as well as in different crystal structures of the E2 state; also the local backbone structure near Glu^{309} varies. In the E2P analog structure of E2(TG+AlF_4^-) (21), the orientation of the backbone carbonyl bond is intermediate between that of the E2(TG) and E2(TG+MgF_4^{2-}) structure, whereas the side chain including the C_α-C_β bond orients similar to the E2(TG) structure. In the E2(CPA+MgF_4^{2-}) structure (32), a further E2P analog, the backbone carbonyl orients as in E2(TG) but the side chain orients inward as in E2(TG+MgF_4^{2-}). Backbone and side-chain orientation of Glu^{309} in E2 structures other than the E2(TG) structure by Toyoshima and Nomura (20), i.e., the E2(TG) structure by Jensen et al. (24), the E2(TG+BHQ) (23), E2(TG)AMPPCP (24), and E2(CPA+ADP) (32) structures, are very similar to those of E2(TG+MgF_4^{2-}). In the case of the E2(TG+BHQ), E2(CPA+MgF_4^{2-}), and E2(CPA+ADP) structures, the inward orientation is probably forced on Glu^{309} because a

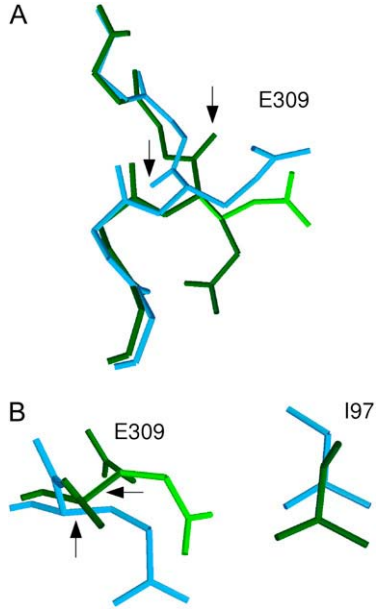

FIGURE 2 The different conformations of the Glu^{309} side chain. (*Blue*) E2(TG) structure (1IWO.pdb) having outwardly oriented Glu^{309}; (*dark green*) the E2(TG+MgF_4^{2-}) structure (1WPG.pdb), having inwardly oriented Glu^{309}; (*light green*) the outwardly oriented, protonated conformer of Glu^{309} from our calculations with E2(TG+MgF_4^{2-}). The hydrogen atoms are omitted for clarity. Structures were overlaid by superposition of the backbone atoms of residues 305–315. (*A*) Side view approximately parallel to the membrane surface. Shown is the backbone of residues 307–311 of M4 and the side chain of Glu^{309}. The conformational change of the backbone around Glu^{309} is clearly seen. The arrows point toward the backbone oxygen of Glu^{309}. (*B*) Top view approximately parallel to M4 toward the lumenal side. Shown are residues Glu^{309} and Ile^{97}. The latter is closest to the outwardly oriented Glu^{309} conformer obtained in our calculations with the E2(TG+MgF_4^{2-}) structure. The arrows point toward the C_α-C_β bond of Glu^{309}, which is oriented differently in the E2(TG) and E2(TG+MgF_4^{2-}) crystal structures. The orientation of this bond is the same for all conformers generated by MCCE with a given backbone structure.

BHQ or CPA molecule occupies the space of the outwardly oriented side chain. Interconversion between inward and outward orientation of Glu^{309} has also been observed in molecular dynamics simulations (Y. Sugita, lecture at the 11th International ATPase Conference 2005, Woods Hole, MA). This survey of protein structures indicates that the backbone structure is variable in E2 and E2P analog states and that the side-chain orientation adopted in the E2P analog structure E2(TG+MgF_4^{2-}) can also be adopted in the E2 state and that of the E2(TG) structure (by Toyoshima and Nomura (20)) can be adopted in E2P analog states.

Glu^{309}: effect of side-chain conformation on calculated pK_a values

We explain the different calculated pK_a values of Glu^{309} obtained with the two E2 structures (Table 2) with the different side-chain conformations generated in our calculations. In E2(TG), Glu^{309} orients predominantly outward and its pK_a was calculated to be 4.7, which is close to that in aqueous

solution. The higher pK_a value calculated for E2(TG+MgF_4^{2-}) (8.4) is not only due to the possibility of the side chain to orient inward but also the outwardly orientated conformer is predominantly protonated at pH 6 and thus it has a higher pK_a than in E2(TG). The outwardly orientated conformers generated with MCCE for E2(TG) and E2(TG+MgF_4^{2-}) are different and their carbonyl carbon atoms are 2.8 Å apart (Fig. 2 *A*). As a consequence, the carboxyl group in E2(TG) comes closer to helix M1, is further away from helix M2, and rises higher up into the channel to the cytoplasm, whereas the E2(TG+MgF_4^{2-}) conformer is more enclosed by, for example, Ile^{97}. This is confirmed by comparison of the calculated reaction field energies $\Delta\Delta G_{rxn}$ of Glu^{309} (see Table S1 of Supplementary Material). $\Delta\Delta G_{rxn}$ is considerably higher in E2(TG+MgF_4^{2-}) than in E2(TG), shifting the reference $pK_{a,sol}$ up by ~2.3 ΔpK_a units in E2(TG+MgF_4^{2-}) versus only 0.9 ΔpK_a units in E2(TG).

The pK_a of Glu^{309} in all E2 states

The above discussion indicates that the pK_a of Glu^{309} in the E2 states varies probably depending on the local backbone structure around Glu^{309}. To estimate which of the conformations is predominantly adopted in E2 states, we have to compare in a first step the calculated free energy values ΔG of Glu^{309} for E2(TG) and E2(TG+MgF_4^{2-}) (Table S1, Supplementary Material). However, these do not contain all relevant contributions, as those from the intrabackbone interactions of the adjacent Gly^{310} residue. These are expected to be different in the two states because the local backbone conformation is different. Therefore we will estimate the strength of the interactions of the peptide group between Glu^{309} and Gly^{310} in a second step. Finally we will incorporate the energy contributions from the intrabackbone interactions into the MCCE-free energy values of Glu^{309} and compare the values for E2(TG) and E2(TG+MgF_4^{2-}).

The free energy values (Table S1, Supplementary Material) indicate that the Glu^{309} side-chain conformation and the interactions of its backbone atoms are more favorable in E2(TG) than in E2(TG+MgF_4^{2-}) by 2.6–2.8 ΔpK_a units between pH 6 and 8. Concerning hydrogen bonding to water, the local backbone conformations around Glu^{309} in E2(TG) and E2(TG+MgF_4^{2-}) seem to be equivalent. The backbone carbonyl oxygen of Glu^{309} in E2(TG+MgF_4^{2-}) is exposed to water. In line with this expectation, a crystal water is found 2.6–2.7 Å from the carbonyl oxygen in the crystal structure of E2(TG+BHQ), which is very similar to that of E2(TG+MgF_4^{2-}) near Glu^{309}. The backbone oxygen of E2(TG)-Glu^{309} is also expected to be hydrogen bonded to a water molecule. The crystal structure does not contain crystal water molecules in its vicinity, but one is placed by the program Dowser (51) at a distance of 2.7 Å.

The NH group of Gly^{310} of E2(TG+MgF_4^{2-}) is expected to be hydrogen bonded because a crystal water molecule at a distance of 2.7 Å is found in the similar E2(TG+BHQ) structure. The NH group of Gly^{310} of E2(TG) is exposed toward the channel and therefore also expected to be hydrogen bonded. Thus, the backbone conformations in E2(TG+MgF_4^{2-}) and E2(TG) both seem to allow for hydrogen bonding of the Glu^{309} C=O and the Gly^{310} NH group with water.

The local intrabackbone interactions around Glu^{309} are more favorable in E2(TG+MgF_4^{2-}) than in E2(TG): in E2(TG+MgF_4^{2-}) there is a hydrogen bond between Gly^{310} NH and Asn^{796} CO, whereas in E2(TG) the two carbonyl groups of Glu^{309} and Asn^{796} repel each other. The latter interaction is included in ΔG_{pol} of Glu^{309} (Table S1, Supplementary Material) as obtained from the MCCE calculation and does not need to be considered separately. An additional difference is the hydrogen bond between the backbone atoms of Pro^{308} and Leu^{311}, which is shorter and better aligned in E2(TG+MgF_4^{2-}). However, this difference seems to be significant only for chains A and D of the E2(TG+MgF_4^{2-}) structure where the O···H distance is 0.5 Å shorter. For chains B and C, the O···H distance is only 0.1 Å shorter. Thus this interaction does not seem to be decisive for the local backbone conformation around Glu^{309} and will not be considered in the following.

Therefore we only had to estimate the energy contribution of the hydrogen bond between Gly^{310} NH and Asn^{796} CO of the local intrabackbone interactions as described in Methods. This intrabackbone hydrogen bond in E2(TG+MgF_4^{2-}) makes the local backbone conformation between Glu^{309} and Gly^{310} ~0.5 ΔpK_a units more favorable in E2(TG+MgF_4^{2-}) than in E2(TG) at $\varepsilon = 4$. We added the interaction energy of −0.5 ΔpK_a units to the ΔG value of Glu^{309} in E2(TG+MgF_4^{2-}) (Table S1, Supplementary Material) to include the hydrogen bond of Gly^{310}. At pH 7.0 we obtained 0.48 ΔpK_a units. The corresponding value for E2(TG) is −1.83 ΔpK_a units. Thus, the E2(TG) conformation of Glu^{309}-Gly^{310} is favorable by 2.1–2.3 ΔpK_a units in the pH range between 6 and 8. This indicates that the E2(TG) backbone structure and the accompanying Glu^{309} side-chain conformations are adopted most of the time for a single ATPase molecule. At any given time, most ATPase molecules in the E2 states adopt the E2(TG) backbone structure around Glu^{309} and have Glu^{309} outwardly orientated as in E2(TG) with a low pK_a (4.7). Some ATPase molecules adopt the E2(TG+MgF_4^{2-}) backbone structure around Glu^{309}, and the Glu^{309} side-chain fluctuates between inward and outward orientations and has a high pK_a (8.4).

Our finding of a predominantly unprotonated Glu^{309} at physiological pH values is supported by mutagenesis studies because mutation of Glu^{309} to Gln slows down dephosphorylation at pH 6.2 (52) and pH 7.0 (14,48). This mutation mimics protonation and should allow dephosphorylation at a rate close to that of the wild-type if Glu^{309} were protonated in E2P.

Low pK_a and high pK_a conformers of Glu^{309} are adopted in different crystal structures, which were all obtained at pH 6.1–6.8 (20,22–24) (J. V. Møller, Aarhus University, private

communication, 2006). The structures were obtained in the presence of inhibitors of which TG is known to stabilize the protonated E2 states (24). In the absence of inhibitors it is therefore expected that the low pK_a conformers of Glu^{309} prevail.

Glu^{309}: summary

Summarizing this discussion about Glu^{309}, our calculations and the x-ray structures give evidence of inwardly and outwardly oriented side-chain conformations of Glu^{309} in the E2(TG) and in the E2(TG+MgF_4^{2-}) state. When Glu^{309} is deprotonated, only the outwardly oriented conformer is occupied. The possibility to orient outward is triggered by the release of Ca^{2+} from its binding sites and less by phosphoenzyme conversion from Ca_2E1P to E2P, as indicated by our calculations with a Ca_2E1P structure where we deleted the two Ca^{2+} from the structure file. The different orientations observed in the crystal structures seem to be physiologically relevant, in line with the proposed role of this residue as a Ca^{2+} gate toward the cytoplasm (17,47,53). The outward orientation of Glu^{309} places it at the end of a water accessible channel toward the cytosol (20) and might be important to guide Ca^{2+} down to the bottom of the channel between the stalk helices S1–S4 before it enters the binding sites. Glu^{309} has the ability to switch between a low pK_a mode ($pK_a = 4.7$) and a high pK_a mode ($pK_a = 8.4$) probably depending on the local backbone conformation. For a given ATPase molecule, our calculations indicate that it will adopt the low pK_a mode most of the time.

Glu^{771}

Our pK_a value for Ca_2E1-Glu^{771} is <0, which is lower than previously calculated (31). Both calculations agree in that Ca_2E1-Glu^{771} is unprotonated at physiological pH and above. In line with that, mutation to Gln strongly reduces the affinity of Ca^{2+}-binding site I as shown by the mM Ca^{2+} concentration needed to inhibit phosphorylation by phosphate (14,48,50,52).

The pK_a of Glu^{771} in the Ca^{2+}-free states was calculated to be larger than 14, indicating that Glu^{771} is protonated. This is in line with a previous calculation on the unphosphorylated Ca^{2+}-free structure E2(TG+BHQ) (23). Mutation to Gln leaves the lumenal low affinity Ca^{2+}-binding sites intact (48) as expected if Glu^{771} is protonated in E2P. On the other hand, this mutation does not allow for fast dephosphorylation of E2P as would be expected if protonation of Glu^{771} were required for dephosphorylation. However, neutralization of Glu^{771} by mutation to Gln does not seem to be the reason for the slow dephosphorylation of E2P because introduction of a positive charge by mutation to Lys makes dephosphorylation nearly as fast as that of the wild-type protein (14). It was concluded (18) that at least two positive charges near Glu^{771} are required for fast E2P dephosphorylation, in line with our calculations that Glu^{771} and the closest residues Asp^{800} and Glu^{908} are protonated.

In light of the accelerating effect of mutation to Lys, the inhibiting effect of mutation to Gln seems to be counterintuitive and does not support the obvious interpretation that E2P-Glu^{771} is ionized. It is possible that Gln is not a good mimic for protonated Glu^{771}. The C=O bond of Glu is stronger than that of Gln, as shown by the higher stretching frequency revealed by infrared spectra in ^2H_2O (54,55) where the vibration is highly localized on this bond. This implies a higher partial charge on the Gln carbonyl oxygen and possibly stronger interactions with the environment. Furthermore, the two hydrogen atoms of Gln might allow for different or additional hydrogen bonds compared to protonated Glu. Since Glu^{771} is at the heart of binding site I, the effects of mutation to Gln might indicate that protonated E2P-Glu^{771} is involved in delicate interactions with its environment, which are important for dephosphorylation.

Asp^{800}

Our calculated pK_a value for Asp^{800} is below 0 in Ca_2E1, 7.9 in E2(TG) (56), and 7.1 and 7.9 in E2(TG+MgF_4^{2-}) with implicit water and five explicitly considered crystal water molecules, respectively. Our result on Asp^{800} for Ca_2E1 agrees well with the pK_a of -4 from a recent calculation (31). However, for the E2 states, our pK_a values of 7–8 in E2(TG) and E2(TG+MgF_4^{2-}) are in contrast to a previous calculation on E2(TG+BHQ), which did not yield a change in protonation state between pH 6 and 8; only a tendency to deprotonate near pH 7 was obtained when ε was set to 20 (23). However, our calculated pK_a values for E2(TG+MgF_4^{2-})-Asp^{800} agree well with experimental data revealing an apparent pK_a of 7.7 for lumenal proton binding to proton countertransporting residues (9) and with the apparent pK_a of 7.2 for proton binding to E2P (57).

The very low pK_a of Asp^{800} in Ca_2E1 correlates with the serious disruption of Ca^{2+}-binding sites by replacing the carboxyl group with an amido group: the mutated ATPase cannot be phosphorylated by ATP in the presence of up to 12.5 mM Ca^{2+} (48). Dephosphorylation of E2P is fast for the Asn mutant (14) at pH 7, in line with Asp^{800} being protonated in E2P. However, dephosphorylation is slow at pH 6.2 (52), which highlights that a straightforward interpretation of mutagenesis results can be difficult.

Glu^{908}

Our calculations indicated a pK_a value for Ca_2E1-Glu^{908} of 3.6 without and 3.7 with explicit water molecules. It is above 14 in E2(TG) and E2(TG+MgF_4^{2-}). In the Ca^{2+}-free states, strong interactions with Asp^{800} seem to prevent deprotonation of Glu^{908} at high pH since the deprotonated Asp^{800} stabilizes the neutral Glu^{908} by more than 4 ΔpK_a units above pH 8 (data not shown). As a result, Glu^{908} deprotonates only partially

above pH 6. Its deprotonation is more pronounced in the calculations with explicit water, where the minimum degree of protonation is 0.73 at pH 9.0 for E2(TG+MgF_4^{2-}) (Table 1).

For Ca_2E1-Glu^{908} our calculated pK_a is the highest pK_a value of the Ca^{2+} ligands in Ca_2E1 but still much lower than pK_a values of >8 ($\varepsilon = 4$) or ~7.5 ($\varepsilon = 20$) that can be inferred from previous calculations (23,31). With side-chain conformations fixed to those in the crystal structure, we calculated a pK_a of 8.3 for Glu^{908} in Ca_2E1 ($\varepsilon = 4$), in close agreement with the cited values. Thus the calculated protonation state of Glu^{908} depends critically on whether or not side-chain mobility is taken into account. This is also reflected in the calculations with fixed side chains by the dependency of the pK_a on the dielectric constant (23). The dielectric constant ε is a macroscopic description of the response of matter on external electric fields, with high ε indicating that the matter contains dipoles that easily adjust their orientation to the electric field. Thus it is not surprising that our multiconformation calculations agree better with the previous results at higher ε.

Our calculations for E2(TG+MgF_4^{2-}) ($pK_a > 14$) agree with previous calculations on E2(TG+BHQ) (23) done at $\varepsilon = 4$ where Glu^{908} is protonated between pH 6 and 8 but not with those at $\varepsilon = 20$ according to which Glu^{908} has a pK_a between 6 and 7. The $\varepsilon = 20$ calculation and our calculation agree in that one of the two nearby residues Asp^{800} or Glu^{908} titrates either Glu^{908}, in the previous calculation, or Asp^{800}, in our calculations. Presumably our MCCE calculations model the protonation state of these strongly coupled residues better, because they allow adjustment of side-chain conformation of one residue to the protonation state of the other.

Mutation of Glu^{908} to Gln has little effect on Ca^{2+} binding (49,52). This seems to indicate that Glu^{908} is protonated in Ca_2E1 or that weaker interactions between Gln^{908} and Ca^{2+} are compensated by other residues. For example, it is conceivable that a hydrogen bond between Gln^{908} and Glu^{771} could pull a second Glu^{771} oxygen into the coordination sphere of Ca^{2+}. It has been concluded that Glu^{908} contributes only one side-chain oxygen to Ca^{2+} binding (52), and it is the only carboxyl residue of the Ca^{2+}-binding sites that is not conserved between Ca^{2+}-ATPase and Na^+/K^+-ATPase (58). Thus it might be less essential than the other carboxyl groups in the binding site. Mutation of Glu^{908} to Gln or Ala allows E2P to decay as fast as the wild-type enzyme (14,52), indicating that Glu^{908} is protonated in E2P, in line with our calculations, or that the Glu^{908} side chain is not important for dephosphorylation.

H^+/Ca^{2+} stoichiometry

For comparison with our calculations, we discuss now experimental data on the number of protons involved in Ca^{2+} binding and proton countertransport. Two (7,10–13,59) or three (57) H^+ are released when the two Ca^{2+} bind to the unphosphorylated ATPase at pH 6. The interpretations differ as to whether each Ca^{2+} competes with 1 H^+ (11–13) or whether the protons have to be released before the first Ca^{2+} binds (10,13,57,59). The latter is often interpreted as the E2 → E1 transition of the Ca^{2+}-free enzyme (10,13,59). Both models have been suggested to operate for different pools of the ATPase molecules (13). Additionally, one (10) or two (12) protons modulate Ca^{2+} binding but do not compete directly with Ca^{2+}. There seems to be no proton uptake or release in the Ca_2E1 → Ca_2E1P reaction (60), but 2–3 H^+ bind to E2P at pH 6 (57,59–61). These numbers suggest that the Ca^{2+} ligands are partly protonated in Ca_2E1 and Ca_2E1P or partly unprotonated in E2P.

According to our calculations, Glu^{309} is predominantly unprotonated at physiological pH values and Asp^{800} is partially unprotonated in E2(TG+MgF_4^{2-}) at higher pH. To obtain calculated H^+/Ca^{2+} stoichiometries at different pH values, we added the fractional protonation values (% protonation/100) of the four acidic Ca^{2+} ligands and subtracted the resulting values for E2(TG+MgF_4^{2-}) from those for Ca_2E1 (Table 1 *A*). Without Glu^{309} we obtained similar numbers of protons that are exchanged for the two Ca^{2+} as the experiments: 2.8 (1.00 + 0.82 + 0.98 − 0.03) at pH 6.0 and 2.4 at pH 7.0. These values will be modulated by other protonatable residues, in particular Glu^{58}, which is protonated in Ca_2E1 but largely unprotonated in E2(TG+BHQ) (23). The respective numbers at pH 8 cannot be compared to Ca^{2+}-binding experiments because the initial state in these is E1, which has lost protons in the E2 → E1 transition.

Residues involved in proton countertransport

Regarding the number of countertransported protons, quantitative measurements indicate that 2–3 H^+ are countertransported per ATPase cycle (6,7,9,61,62). Furthermore, electrogenicity of the Ca^{2+}-ATPase was directly demonstrated by measuring a stationary current (63), ruling out that 4 H^+ are countertransported.

At pH 6 our calculations indicate that Glu^{771}, Asp^{800}, and Glu^{908} are protonated in the E2 states, whereas Glu^{309} is predominantly unprotonated. Assuming participation of Glu^{771}, Asp^{800}, and Glu^{908} but not of Glu^{309} in proton countertransport, the data in Table 1 *A* for E2(TG+MgF_4^{2-}) suggest the following numbers of countertransported protons per cycle (per 2 Ca^{2+}) near the physiological pH value—2.8 at pH 6 and 2.4 at pH 7—in close agreement with the experimental values of 2–3.

We exclude Glu^{309} from being a residue that binds countertransported protons in the E2 states, not only because of its low pK_a value but also because of the conformational heterogeneity of its side chain: when Ca^{2+} dissociates from site II, Glu^{309} is left ionized and its side chain has the tendency to move outward as shown here. If this is faster than protonation from the lumen, Glu^{309} will receive a proton from the cytoplasmic side and not from the lumenal side and will therefore not participate in proton countertransport even if Glu^{309} were protonated in the E2 states.

Glu^{309} might nevertheless play a role in proton countertransport: protons released upon Ca^{2+} binding to binding site I could be (partially) taken up by Glu^{309} and then transferred to the cytoplasm. Thus Glu^{309} could serve as a proton shuttle between the Ca^{2+}-binding site and cytoplasm.

It has been mentioned before that Glu^{58} might receive a proton from Glu^{309} when Ca^{2+} binds to the unphosphorylated enzyme (23). Since we favor the view that Glu^{309} receives its proton from the cytoplasmic side, we consider a role of Glu^{58} in proton countertransport as unlikely. Furthermore, the proximity of Glu^{58} and Glu^{309} in the structure of Ca_2E1 seems to be characteristic only for this state. In all available structures of the nucleotide-bound state in the presence (53,64) and absence (24,32) of Ca^{2+}, of a Ca_2E1P analog (22,64), of E2P analogs (21,22,32), and of E2(TG) (20,24), the C_α-C_β bond and the side chain of Glu^{58} point away from Glu^{309}. This raises questions regarding proton transfer between Glu^{309} and Glu^{58} under physiological conditions of high ATP concentrations where an ATP-free Ca_2E1 state is bypassed (65) and closed conformations are adopted throughout the catalytic cycle (24).

At high pH, the data in Table 1 *A* suggest 2.1 (pH 8) and 2.0 (pH 9) countertransported protons per cycle (per 2 Ca^{2+}). These numbers are larger than experimental values at high pH. This discrepancy at high pH is due to Glu^{771} and Glu^{908}, which have calculated pK_a values that are much higher than the apparent experimental value near 7.5 for lumenal proton binding of countertransported protons (9,57,59). However, the high pK_a values of Glu^{771} and Glu^{908} in our calculations do not per se exclude their involvement in proton countertransport. Since they are protonated in E2 states but are unprotonated in Ca_2E1 at pH 7, they lose their proton upon Ca^{2+} binding. Several scenarios can explain the discrepancy between their calculated high pK_a values and the apparent experimental pK_a value of proton countertransporting residues in E2P:

1. There could be a pH-dependent switch of proton pathways, caused for example by deprotonation of Asp^{800}, making proton uptake and release vectorial at low pH but not at high pH. This could make Glu^{771} and Glu^{908} participate in proton countertransport at low pH but not at high pH, although they become protonated upon Ca^{2+} release at all studied pH values.
2. A pH-dependent conformational change possibly caused by deprotonation of Asp^{800} could make the E2(TG+MgF_4^{2-}) structure, which was obtained at pH 6.1, inappropriate for calculations at high pH. The conformational side-chain flexibility implemented in MCCE reduces but does not eliminate the dependence on the initial structure.
3. The pK_a values of Glu^{771} and Glu^{908} could be lower than calculated because of nearby hydronium ions, only partial Ca^{2+} release, or binding of positive ions other than H^+ to the Ca^{2+}-binding site, promoted by the higher affinity of the Ca^{2+}-binding sites at high pH (59,66,67) or because of a more open Ca^{2+}-release pathway in genuine E2P as compared to E2(TG+MgF_4^{2-}). The latter would allow more water molecules to penetrate the transmembrane region, which will decrease the pK_a values of the acidic Ca^{2+} ligands.

Ca^{2+} release path in E2P

The flexibility of the Glu^{309} side chain not only supports a Ca^{2+}-gating function of this residue toward the cytoplasm, it might also be important for the release of Ca^{2+} from the phosphoenzyme to the SR lumen. Ca^{2+} release is likely to be triggered by an outward movement of the Glu^{309} side chain away from the Ca^{2+}-binding sites. This movement could pull Ca^{2+} at binding site II into a cavity under the Glu^{309} side chain and away from the Ca^{2+} exit channel proposed by Toyoshima et al. (22). Exit to the cytoplasmic side is blocked by the outwardly oriented Glu^{309} side chain together with those of Ile^{307} and Leu^{65} and the backbone of Pro^{308}. Exit to the lumen seems to be possible by a channel that is mainly formed by residues in transmembrane helices M1, M2, and M4 and runs parallel to the one proposed earlier (22) on the ''other side'' of Val^{304} closer to transmembrane helices M1 and M2. The Ca^{2+} exit channel proposed by us is shown in Fig. 3, and structural details of it are discussed in the Supplementary Material.

A continuous channel is generated when the molecular surface of the channel-lining residues is calculated with a

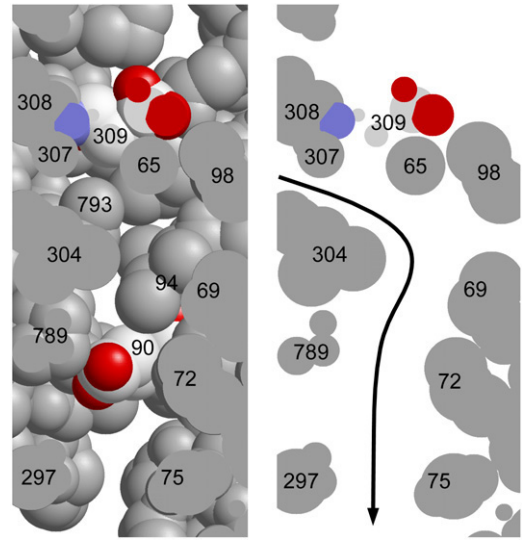

FIGURE 3 The suggested Ca^{2+} release path between transmembrane helices M1, M2, and M4. Shown is the suggested Ca^{2+} exit path within the membrane domain of the E2(TG+AlF_4^-) structure (21) in van der Waals representation viewed approximately parallel to the membrane surface. The left-hand side shows a cut through the structure and the right-hand side a slice of the structure. The arrow indicates the Ca^{2+} path. Residue numbers are given for a selection of residues. Two glutamic acids are highlighted by cpk colors.

sphere radius of 1.2 Å and smaller, indicating that a sphere of the radius of Ca^{2+} (1.0 Å) (68) can pass the exit channel if Ca^{2+} passes without hydration shell. However, this is unlikely since only the oxygens of Ala^{68} and Val^{300} provide favorable interactions in the outlet channel together with one of the carboxyl oxygens of Glu^{90} when it orients upward. The charge of the Glu^{90} side chain reduces the net charge in the outlet channel to +1. Then the three oxygens provided for Ca^{2+} can be compared to the eight oxygen ligands provided for each K^+ in the selectivity filter of K^+ channels in which K^+ is dehydrated (assuming an average occupancy of two of the four binding sites) (69). Therefore the small number of oxygens in the Ca^{2+} exit channel makes it unlikely that Ca^{2+} passes without its hydration shell. Given that the radius of hydrated Ca^{2+} is 4.1 Å (68), we consider the exit channel as closed in the E2P analog structures, in line with experimental data (21,45,70). For the limiting case of a hydrophobic channel, a radius of ~6.5 Å is required to allow the monovalent cation Na^+ to pass according to molecular simulations (71).

Most of the steric constraints of the Ca^{2+} channel are between transmembrane helices M1 and M4 or M2 and M4. This implies that the channel can be opened and closed by movements of helices M1 and M2 relative to M3 and M4. The inhibitor TG blocks lumenal access of Ca^{2+} to the binding sites (45). Since TG binds to transmembrane helices M3–M5 and M7, it cross-links M3 and M4 to the C-terminal portion of the membrane domain and could thus block movement relative to M1 and M2, which is required to open the exit channel.

Movements of transmembrane helices M1 and M2 relative to M3 and M4 are a recurring theme in the structural reorganizations that take place during Ca^{2+} pumping. In Ca_2E1, M1 and M2 have moved down toward the SR lumen with respect to M3 and M4 and adopt a different position with respect to M4. This disrupts the Ca^{2+} exit path. Between helices M4 and M6 a small cavity is formed in Ca_2E1 close to the Ca^{2+} site II, and between M1, M2, and M4 a larger cavity is formed farther down toward the SR lumen (between Leu^{65}, Ile^{94}, Lys^{297}, Pro^{789}, and Val^{790}). Contact between the small cavity and Ca^{2+} is prevented by Val^{304}, Ala^{305}, and Asn^{796}, and contact to the larger cavity is blocked by Leu^{65}, Ala^{301}, Leu^{792}, and Leu^{793}.

CONCLUSIONS

Taking together our calculations and previous experimental findings, we propose that Glu^{771}, Asp^{800}, and Glu^{908} bind protons in E2P(TG+MgF_4^{2-}) and lose them upon Ca^{2+} binding to the unphosphorylated enzyme. They are prime candidates for the proton countertransporting residues. These residues are part of Ca^{2+}-binding site I and are thus likely to receive and release their proton via the same path. Binding of lumenal protons by Glu^{309} in E2P(TG+MgF_4^{2-}) is questionable because its conformational flexibility allows contact to the cytosol. Instead, it might serve as a proton shuttle between Ca^{2+}-binding site I and the cytoplasm. Without the participation of Glu^{309}, our calculated number of countertransported residues is between 2 and 3, which compares favorably with experimental values at physiological pH and below. Outward movement of the Glu^{309} side chain is a possible trigger for Ca^{2+} release along an exit path between transmembrane helices M1, M2, and M4.

SUPPLEMENTARY MATERIAL

To view all of the supplemental files associated with this article, visit www.biophysj.org.

We thank Marilyn Gunner (City College of New York) for providing us with the MCCE code, Christian Weidemüller (Universität Frankfurt, Germany) for preparation of Fig. 1 and setup of the membrane for control calculations, and Eeva-Liisa Karjalainen (Stockholm University, Sweden) for applying the program Dowser (51) to the crystal structures.

The work was supported by the Deutsche Forschungsgemeinschaft (SFB 472).

REFERENCES

1. Hasselbach, W., and M. Makinose. 1961. The calcium pump of the relaxing granules of muscle and its dependence on ATP splitting. *Biochem. Z.* 333:518–528.
2. Mintz, E., and F. Guillain. 1997. Ca^{2+} transport by the sarcoplasmic reticulum ATPase. *Biochim. Biophys. Acta.* 1318:52–70.
3. Toyoshima, C., and G. Inesi. 2004. Structural basis of ion pumping by Ca^{2+}-ATPase of the sarcoplasmic reticulum. *Annu. Rev. Biochem.* 73: 269–292.
4. Stokes, D. L., and N. M. Green. 2003. Structure and function of the calcium pump. *Annu. Rev. Biophys. Biomol. Struct.* 32:445–468.
5. Lee, A., and J. East. 2001. What the structure of a calcium pump tells us about its mechanism. *Biochem. J.* 356:665–683.
6. Levy, D., M. Seigneuret, A. Bluzat, and J. L. Rigaud. 1990. Evidence for proton countertransport by the sarcoplasmic reticulum Ca^{2+}-ATPase during calcium transport in reconstituted proteoliposomes with low ionic permeability. *J. Biol. Chem.* 265:19524–19534.
7. Chiesi, M., and G. Inesi. 1980. Adenosine 5′-triphosphate dependent fluxes of manganese and hydrogen ions in sarcoplasmic reticulum vesicles. *Biochemistry.* 19:2912–2928.
8. Da Costa, A. G., and V. M. C. Madeira. 1994. Proton ejection as a major feature of the Ca^{2+}-pump. *Biochim. Biophys. Acta.* 1189: 181–188.
9. Yu, X., L. N. Hao, and G. Inesi. 1994. A pK_a change of acidic residues contributes to cation countertransport in the Ca-ATPase of sarcoplasmic reticulum. Role of H^+ in Ca^{2+}-ATPase countertransport. *J. Biol. Chem.* 269:16656–16661.
10. Forge, V., E. Mintz, and F. Guillain. 1993. Ca^{2+} binding to sarcoplasmic reticulum ATPase revisited. I. Mechanism of affinity and cooperativity modulation by H^+ and Mg^{2+}. *J. Biol. Chem.* 268:10953–10960.
11. Martin, R. B. 1992. Cooperative proton and calcium binding by sarcoplasmic reticulum ATPase. *FEBS Lett.* 308:59–61.
12. Froud, R. J., and A. G. Lee. 1986. Conformational transitions in the Ca^{2+} + Mg^{2+}-activated ATPase and the binding of Ca^{2+} ions. *Biochemistry.* 237:197–206.
13. Nakamura, J. 1994. Two types of proton-modulated calcium binding in the sarcoplasmic reticulum Ca^{2+}-ATPase. II. Characteristics of their calcium bindings. *J. Biol. Chem.* 269:30822–30827.

14. Andersen, J. P. 1995. Dissection of the functional domains of the sarcoplasmic reticulum Ca^{2+}-ATPase by site-directed mutagenesis. *Biosci. Rep.* 15:243–261.
15. Toyoshima, C., M. Nakasako, H. Nomura, and H. Ogawa. 2000. Crystal structure of the calcium pump of sarcoplasmic reticulum at 2.6 Å resolution. *Nature.* 405:647–655.
16. Vilsen, B., and J. P. Andersen. 1992. Mutational analysis of the role of Glu^{309} in the sarcoplasmic reticulum Ca^{2+}-ATPase of frog skeletal muscle. *FEBS Lett.* 306:247–250.
17. Vilsen, B., and J. P. Andersen. 1998. Mutation to the glutamate in the fourth membrane segment of Na^+, K^+-ATPase and Ca^{2+}-ATPase affects cation binding from both sides of the membrane and destabilizes the occluded enzyme forms. *Biochemistry.* 37:10961–10971.
18. Andersen, J. P. 1994. Mutational analysis of Glu^{771} of the Ca^{2+}-ATPase of sarcoplasmic reticulum. Effect of positive charge on dephosphorylation. *FEBS Lett.* 354:93–96.
19. Andersen, J. P., and B. Vilsen. 1994. Amino acids Asn^{796} and Thr^{799} of the Ca^{2+}-ATPase of sarcoplasmic reticulum bind Ca^{2+} at different sites. *J. Biol. Chem.* 269:15931–15936.
20. Toyoshima, C., and H. Nomura. 2002. Structural changes in the calcium pump accompanying the dissociation of calcium. *Nature.* 418: 605–611.
21. Olesen, C., T. L.-M. Sørensen, R. C. Nielsen, J. V. Møller, and P. Nissen. 2004. Dephosphorylation of the calcium pump coupled to counterion occlusion. *Science.* 306:2251–2255.
22. Toyoshima, C., H. Nomura, and T. Tsuda. 2004. Lumenal gating mechanism revealed in calcium pump crystal structures with phosphate analogues. *Nature.* 432:361–368.
23. Obara, K., N. Miyashita, C. Xu, I. Toyoshima, Y. Sugita, G. Inesi, and C. Toyoshima. 2005. Structural role of countertransport revealed in Ca^{2+} pump crystal structure in the absence of Ca^{2+}. *Proc. Natl. Acad. Sci. USA.* 102:14489–14496.
24. Jensen, A. M. L., T. L. M. Sørensen, C. Olesen, J. V. Møller, and P. Nissen. 2006. Modulatory and catalytic modes of ATP binding by the calcium pump. *EMBO J.* 25:2305–2314.
25. Buchet, R., I. Jona, and A. Martonosi. 1991. Ca^{2+} release from caged-Ca^{2+} alters the FTIR spectrum of sarcoplasmic reticulum. *Biochim. Biophys. Acta.* 1069:209–217.
26. Barth, A., W. Mäntele, and W. Kreutz. 1997. Ca^{2+} release from the phosphorylated and the unphosphorylated sarcoplasmic reticulum Ca^{2+} ATPase results in parallel structural changes. An infrared spectroscopic study. *J. Biol. Chem.* 272:25507–25510.
27. Georg, H., A. Barth, W. Kreutz, F. Siebert, and W. Mäntele. 1994. Structural changes of sarcoplasmic reticulum Ca^{2+} ATPase upon Ca^{2+} binding studied by simultaneous measurement of infrared absorbance changes and changes of intrinsic protein fluorescence. *Biochim. Biophys. Acta.* 1188:139–150.
28. Barth, A. 1999. Phosphoenzyme conversion of the sarcoplasmic reticulum Ca^{2+}-ATPase. Molecular interpretation of infrared difference spectra. *J. Biol. Chem.* 274:22170–22175.
29. Barth, A., W. Kreutz, and W. Mäntele. 1994. Changes of protein structure, nucleotide microenvironment, and Ca^{2+} binding states in the catalytic cycle of sarcoplasmic reticulum Ca^{2+} ATPase: investigation of nucleotide binding, phosphorylation and phosphoenzyme conversion by FTIR difference spectroscopy. *Biochim. Biophys. Acta.* 1194: 75–91.
30. Troullier, A., K. Gerwert, and Y. Dupont. 1996. A time-resolved Fourier transformed infrared difference spectroscopy study of the sarcoplasmic reticulum Ca^{2+}-ATPase: kinetics of the high-affinity calcium binding at low temperature. *Biophys. J.* 71:2970–2983.
31. Sugita, Y., N. Miyashita, M. Ikeguchi, A. Kidera, and C. Toyoshima. 2005. Protonation of the acidic residues in the transmembrane cation-binding sites of the Ca^{2+} pump. *J. Am. Chem. Soc.* 127:6150–6151.
32. Moncoq, K., C. A. Trieber, and H. S. Young. 2007. The molecular basis for cyclopiazonic acid inhibition of the sarcoplasmic reticulum calcium pump. *J. Biol. Chem.* 282:9748–9757.
33. Georgescu, R. E., E. G. Alexov, and M. R. Gunner. 2002. Combining conformational flexibility and continuum electrostatics for calculating pK_as in proteins. *Biophys. J.* 83:1731–1748.
34. Alexov, E. G., and M. R. Gunner. 1997. Incorporating protein conformational flexibility into the calculation of pH-dependent protein properties. *Biophys. J.* 72:2075–2093.
35. Nicholls, A., and B. Honig. 1991. A rapid finite-difference algorithm, utilizing successive over-relaxation to solve the Poisson-Boltzmann equation. *J. Comput. Chem.* 12:435–445.
36. Sitkoff, D., K. A. Sharp, and B. Honig. 1994. Accurate calculation of hydration-free energies using macroscopic solvent models. *J. Phys. Chem.* 98:1978–1988.
37. Hauser, K., J. Mao, and M. R. Gunner. 2004. pH dependence of heme electrochemistry in cytochromes investigated by multiconformation continuum electrostatic calculations. *Biopolymers.* 74:51–54.
38. Haas, A. H., and C. R. D. Lancaster. 2004. Calculated coupling of transmembrane electron and proton transfer in dehemic quinol:fumerate reductase. *Biophys. J.* 87:4298–4315.
39. Mao, J., K. Hauser, and M. R. Gunner. 2003. How cytochromes with different folds control heme redox potentials. *Biochemistry.* 42:9829–9840.
40. Song, Y., J. Mao, and M. R. Gunner. 2006. Electrostatic environment of hemes in proteins: pK_as of hydroxyl ligands. *Biochemistry.* 45: 7949–7958.
41. Kim, J., J. Mao, and M. R. Gunner. 2005. Are acidic and basic groups in buried proteins predicted to be ionized? *J. Mol. Biol.* 348:1283–1298.
42. Murzin, A. G., S. E. Brenner, T. Hubbard, and C. Chothia. 1995. SCOP—a structural classification of proteins database for the investigation of sequences and structures. *J. Mol. Biol.* 247:536–540.
43. Buck, M., and M. Karplus. 2001. Hydrogen bond energetics: a simulation and statistical analysis of *N*-methyl acetamide (NMA), water, and human lysozyme. *J. Phys. Chem. B.* 105:11000–11015.
44. Martz, E. 2002. Protein explorer: easy yet powerful macromolecular visualization. *Trends Biochem. Sci.* 27:107–109.
45. Picard, M., C. Toyoshima, and P. Champeil. 2006. Effects of inhibitors on luminal opening of Ca^{2+} binding sites in an E2P-like complex of sarcoplasmic reticulum Ca^{2+}-ATPase with Be^{2+}-fluoride. *J. Biol. Chem.* 281:3360–3369.
46. Clarke, D. M., T. W. Loo, G. Inesi, and D. H. MacLennan. 1989. Location of high affinity Ca^{2+} binding sites within the predicted transmembrane domain of the sarcoplasmic reticulum Ca^{2+}-ATPase. *Nature.* 339:476–478.
47. Inesi, G., H. Ma, D. Lewis, and C. Xu. 2004. Ca^{2+} occlusion and gating function of Glu^{309} in the ADP-fluoroaluminate analog of the Ca^{2+}-ATPase phosphoenzyme intermediate. *J. Biol. Chem.* 279: 31629–31637.
48. Andersen, J. P., and B. Vilsen. 1992. Functional consequences of alterations to Glu^{309}, Glu^{771}, and Asp^{800} in the Ca^{2+}-ATPase of sarcoplasmic reticulum. *J. Biol. Chem.* 267:19383–19387.
49. Clarke, D. M., T. W. Loo, and D. H. MacLennan. 1990. Functional consequences of alterations to polar amino acids located in the transmembrane domain of the Ca^{2+}-ATPase of sarcoplasmic reticulum. *J. Biol. Chem.* 265:6262–6267.
50. Strock, C., M. Cavagna, W. E. Peiffer, C. Sumbilla, D. Lewis, and G. Inesi. 1998. Direct demonstration of Ca^{2+} binding defects in sarcoendoplasmic reticulum Ca^{2+} ATPase mutants overexpressed in COS-1 cells transfected with adenovirus vectors. *J. Biol. Chem.* 273:15104–15109.
51. Zhang, L., and J. Hermans. 1996. Hydrophilicity of cavities in proteins. *Proteins.* 24:433–438.
52. Chen, L., C. Sumbilla, D. Lewis, L. Zhong, C. Strock, M. E. Kirtley, and G. Inesi. 1996. Short and long range functions of amino acids in the transmembrane region of the sarcoplasmic reticulum ATPase. *J. Biol. Chem.* 271:10745–10752.
53. Toyoshima, C., and T. Mizutani. 2004. Crystal structure of the calcium pump with a bound ATP analogue. *Nature.* 430:529–535.

54. Barth, A. 2000. The infrared absorption of amino acid side chains. *Prog. Biophys. Mol. Biol.* 74:141–173.

55. Chirgadze, Y. N., O. V. Fedorov, and N. P. Trushina. 1975. Estimation of amino acid residue side chain absorption in the infrared spectra of protein solutions in heavy water. *Biopolymers.* 14:679–694.

56. Hauser, K. 2006. Electrostatic calculations for assignment of IR difference bands to carboxyl groups getting protonated during protein reactions. *Biopolymers.* 82:430–434.

57. Peinelt, C., and H. J. Apell. 2002. Kinetics of the Ca^{2+}, H^+, and Mg^{2+} interaction with the ion-binding sites of the SR Ca-ATPase. *Biophys. J.* 82:170–181.

58. Andersen, J. P., and B. Vilsen. 1998. Structure-function relationships of the calcium binding sites of the sarcoplasmic reticulum Ca^{2+}-ATPase. *Acta Physiol. Scand.* 163:45–54.

59. Tadini-Buoninsegni, F., G. Bartolommei, M. R. Moncelli, R. Guidelli, and G. Inesi. 2006. Pre-steady state electrogenic events of Ca^{2+}/H^+ exchange and transport by the Ca^{2+}-ATPase. *J. Biol. Chem.* 281: 37720–37727.

60. Yamaguchi, M., and T. Kanazawa. 1985. Coincidence of H^+ binding and Ca^{2+} dissociation in the sarcoplasmic reticulum Ca-ATPase during ATP hydrolysis. *J. Biol. Chem.* 260:4896–4900.

61. Buoninsegni, F. T., G. Bartolommei, M. R. Moncelli, G. Inesi, and R. Guidelli. 2004. Time-resolved charge translocation by sarcoplasmic reticulum Ca-ATPase measured on a solid supported membrane. *Biophys. J.* 86:3671–3686.

62. Yu, X., S. Carrol, J.-L. Rigaud, and G. Inesi. 1993. H^+ countertransport and electrogenicity of the sarcoplasmic reticulum Ca^{2+} pump in reconstituted proteoliposomes. *Biophys. J.* 64:1232–1242.

63. Hartung, K., E. Grell, W. Hasselbach, and W. Bamberg. 1987. Electrical pump currents generated by the Ca^{2+}-ATPase of sarcoplasmic reticulum vesicles absorbed on black lipid membranes. *Biochim. Biophys. Acta.* 900:209–220.

64. Sørensen, T. L.-M., J. V. Møller, and P. Nissen. 2004. Phosphoryl transfer and calcium ion occlusion in the calcium pump. *Science.* 304: 1672–1675.

65. Stahl, N., and W. P. Jencks. 1987. Reactions of the sarcoplasmic reticulum calcium adenosinetriphosphatase with ATP and Ca^{2+} that are not satisfactorily described by an E_1-E_2 model. *Biochemistry.* 26: 7654–7667.

66. Verjovski-Almeida, S., and L. De Meis. 1977. pH-induced changes in the reactions controlled by the low- and high-affinity Ca^{2+}-binding sites in sarcoplasmic reticulum. *Biochemistry.* 16:329–334.

67. Forge, V., E. Mintz, D. Canet, and F. Guillain. 1995. Lumenal Ca^{2+} dissociation from the phosphorylated Ca^{2+}-ATPase of the sarcoplasmic reticulum is sequential. *J. Biol. Chem.* 270:18271–18276.

68. Israelachvili, J. N. 1992. Intermolecular and Surface Forces. Academic Press, London. 55.

69. MacKinnon, R. 2003. Potassium channels. *FEBS Lett.* 555:62–65.

70. Danko, S., K. Yamasaki, T. Daiho, and H. Suzuki. 2004. Distinct natures of beryllium fluoride-bound, aluminum fluoride-bound, and magnesium fluoride-bound stable analogues of an ADP-insensitive phosphoenzyme intermediate of sarcoplasmic reticulum Ca^{2+}-ATPase. *J. Biol. Chem.* 279:14991–14998.

71. Beckstein, O., P. C. Biggin, P. Bond, J. N. Bright, C. Domene, A. Grottesi, J. Holyoake, and M. S. P. Sansom. 2003. Ion channel gating: insights via molecular simulations. *FEBS Lett.* 555:85–90.